Chinese Physics B

A cluster calculation investigation of the A- and B-sites ordered perovskite oxide $CaCu_3Fe_2Os_2O_{12}$

To cite this article before publication: Xiao Wang *et al* 2025 *Chinese Phys. B* in press https://doi.org/10.1088/1674-1056/ae1204

A cluster calculation investigation of the A- and B-sites ordered perovskite oxide $CaCu_3Fe_2Os_2O_{12}$

Xiao Wang(王潇)[1,2,†], Stefano Agrestini[3], Arata Tanaka[4], Zhiwei Hu(胡志伟)[5,†], and Youwen Long(龙有文)[2,†]

[1]*Institute of Quantum Materials and Physics, Henan Academy of Sciences, Zhengzhou, 450046, China*
[2]*Beijing National Laboratory for Condensed Matter Physics, Institute of Physics, Chinese Academy of Sciences, Beijing 100190, China*
[3]*Diamond Light Source, Harwell Campus, Didcot, OX11 0DE, UK*
[4]*Quantum Matter Program, Graduate School of Advanced Science and Engineering, Hiroshima University, Higashi-Hiroshima 739-8530, Japan*
[5]*Max Planck Institute for Chemical Physics of Solids, Dresden 01187, Germany*

Taking the quadruple perovskite oxide $CaCu_3Fe_2Os_2O_{12}$ as an example, by performing both experimental sum rules and theoretical configuration interaction cluster calculations, we have investigated the spin and orbital configurations of all the transition metal cations, Cu, Fe and Os, as well as their local microscopic physical parameters of crystal field, spin-orbit coupling (SOC), Coulomb potential and hybridization. Specially, we found that the Os^{5+} ($5d^3$) with a half-filled t_{2g} orbital exhibits a large orbital moment on account of the mixing of t_{2g} and e_g orbitals, which can be ascribed to the strong SOC of the 5*d* elements. On the other hand, SOC of the Cu^{2+} ($3d^9$) is markedly reduced, but is still nonnegligible compared to the crystal field 10*Dq*, leading to a finite orbital moment of Cu^{2+}. This work provides a microscopic and element-selective perspective of the local environment of the magnetic cations in complex compounds.

Keywords: cluster calculation, X-ray magnetic circular dichroism, spin-orbit coupling, crystal field

PACS: 31.15.am, 75.10.Dg, 75.70.Tj, 87.64.ku

1. Introduction

The A- and B-site ordered perovskite oxide $AA'_3B_2B'_2O_{12}$ has attracted much attention due to the flexibility of accommodating multiple transition metals (TMs) at all A, A', B and B' sites. The strong and complex magnetic and electric correlations can lead to various intriguing physical properties such as charge ordering,[1–4] multiferroicity,[5–7] metal-insulator transition,[8] colossal magnetoresistivity,[9] half-metallicity[10–12] and catalysis.[13–15]

$CaCu_3Fe_2Os_2O_{12}$ (CCFOO)[16] is one of the pioneering studies of A- and B-site ordered perovskite oxides with intricate electronic and magnetic couplings. As shown

† Corresponding author. E-mail: xwang@hnas.ac.cn
† Corresponding author. E-mail: zhiwei.hu@cpfs.mpg.de
† Corresponding author. E-mail: ywlong@iphy.ac.cn

in Fig. 1, the Ca and Cu orderly occupy the A and A' sites respectively with an 1:3 ratio, and Fe and Os reside at the B and B' sites respectively in a rock-salt order. The A′O_4 square planar and B/B′O_6 octahedron units are connected via the corner-shared O atoms. Different from traditional ABO_3 perovskite with canonical intra-site B-B magnetic interaction, first principle calculations indicates that the inter-site magnetic coupling between the A'-site Cu and B'-site Os dominates thus resulting a very high Curie temperature of 580 K with a $Cu^{2+}(\uparrow)Fe^{3+}(\uparrow)Os^{5+}(\downarrow)$ valence and spin configuration which was proved by the element selective X-ray absorption spectroscopic (XAS) and X-ray magnetic circular dichroic (XMCD) measurements.[17]

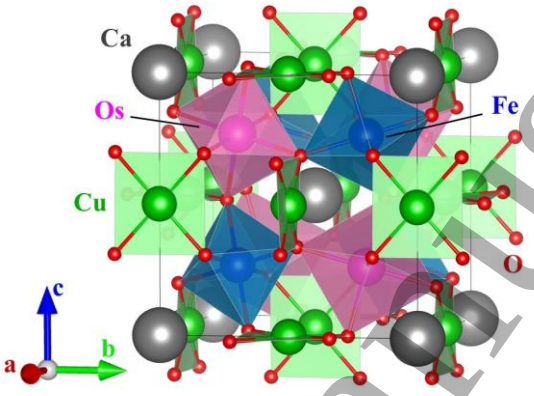

Fig. 1. Crystal structure of $CaCu_3Fe_2Os_2O_{12}$.

In general, the single occupation of the *d* orbital for $Cu^{2+}(3d^9)$, either the half-filled *d* orbital for Os^{5+} (t_{2g}^3), do not carry any orbital moment. However, we noticed that for both Cu^{2+} and Os^{5+} in CCFOO, the XMCD intensities at the L_3 and L_2 edges are not equal,[16,17] leading to a nonzero integration, as an indication of nonnegligible orbital moments that are not expected.[18,19] Interestingly, this nonzero orbital contribution was observed in many other similar perovskite oxides [10–12,20,21]. For example, in $ACu_3Fe_2Re_2O_{12}$ (A = Ca and La), orbital moments of 0.04~0.06 μ_B/Cu were observed.[10,12] Nevertheless, the origin still remains unsolved. On the other hand, for the 5*d* TMs, an extreme large spin-orbit coupling (SOC) can lead to mixing of the occupied and unoccupied orbitals, resulting in large orbital moment.[22–24] For example, in Sr_2IrO_4 and $CaCu_3Ir_4O_{12}$, Ir^{4+} ($5d^5$) forms a $J_{eff} = 1/2$ state with a large L_z/S_z of 4.[25–27] Therefore in CCFOO, which accommodate 3*d* Cu^{2+} with single hole and 5*d* Os^{5+} with fully occupied spin up state, acts as an appropriate example to study the origin of the L_z and its contribution to total magnetic moment.

In this work, we carry out XMCD study of CCFOO by performing both experimental sum rules and theoretical configuration interaction (CI) cluster calculations, obtain the microscopic physical parameters such as crystal field, SOC, Coulomb potential and hybridization, of all the three transition metals, and investigate the origin of the orbital moments of Os^{5+} and Cu^{2+}. We found that a nonnegligible SOC compared to the crystal field can result in some mixing of the t_{2g} and e_g orbitals, thus generating a nonzero orbital moment.

2. Methods

The sum rules,[18,19] which can not only figure out the spin-spin coupling among them, but also can obtain the spin and orbital moments separately,[28–30] were carried out using the following equations

$$m_{orb} = -\frac{4\int_{L_3+L_2}(\mu^+ - \mu^-)d\omega}{3\int_{L_3+L_2}(\mu^+ + \mu^-)d\omega}(10 - n_d), \quad (1)$$

$$m_{spin} + 7\langle T_z\rangle = -\frac{2\int_{L_3}(\mu^+ - \mu^-)d\omega - 4\int_{L_2}(\mu^+ - \mu^-)d\omega}{\int_{L_3+L_2}(\mu^+ + \mu^-)d\omega}(10 - n_d), \quad (2)$$

where m_{orb} and m_{spin} are orbital and spin moments (μ_B/atom), respectively, and n_d is the number of electrons occupying the d orbital of the TM. μ^+ (μ^-) is the XAS with the magnetic field parallel (antiparallel) to the spin of the incident light, and L_3 (L_2) indicates the integrated region. The term $7\langle T_z\rangle$ represents the intra-atomic dipole moment. Note that the $7\langle T_z\rangle$ is negligible for Os^{5+} with O_h symmetry[30–32] and 3d elements[33,34] in current CCFOO.

The CI cluster calculation[35] was performed to investigate the local environment of the TMs in CCFOO. It includes the full intra-atomic multiplet interactions, SOC, the TM d to O-2p hybridization, and the crystal field interaction. This model has very successfully reproduced the line shape of XMCD spectra of 3d, 4d and 5d TM in the past decades.[36–40] The calculations were performed using the XTLS 9.0 code.[41]

3. Results and Discussion

The experimental Cu-, Fe- and Os-$L_{2,3}$ XMCD spectra are taken from Ref. [17] and are depicted in Figs. 2(a), 4(a) and 6(a), respectively. As shown in Fig. 2(a), the XMCD intensity at the Os-L_2 edge is obviously larger than that at the L_3 edge, indicating an unquenched orbital moment of Os^{5+}, which is unexpected for a $5d^3$ configuration. Using the sum rules we obtained orbital and spin moments of 0.16(3) μ_B and −1.52(3) μ_B respectively, as listed in Table 1. The $m_{\mathrm{orb}}/m_{\mathrm{spin}}$ ratio is calculated to be −0.10, indicating a considerable orbital moment of Os^{5+}. It is worth noting that the choices of the edge jump function, background subtraction, and integrating range can result variations for the spin and orbital moments. We have tested different parameters and estimated an error bar of ±0.03 μ_B.

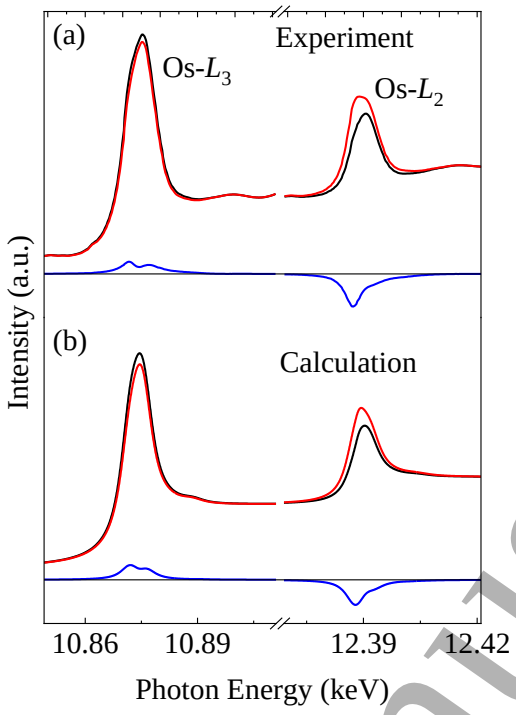

Fig. 2. (a) Experimental and (b) calculated XAS and XMCD spectra at the Os-$L_{2,3}$ edges.

Table 1. Sum rules and CI calculation results of CCFOO.

atom	moment	sum rules	CI calculation
Os (μ_B/atom)	m_{orb}	0.16(3)	0.18
	m_{spin}	−1.52(3)	−2.29
	m_{orb}/m_{spin}	−0.10	−0.08
Cu (μ_B/atom)	m_{orb}	0.06(3)	0.03
	m_{spin}	0.27(3)	0.29
	m_{orb}/m_{spin}	0.22	0.10
Fe (μ_B/atom)	m_{orb}	/	0.007
	m_{spin}	/	4.15
	m_{orb}/m_{spin}	/	0.002
total		/	5.0 μ_B/f.u.

In order to obtain a better understanding of the origin of the unquenched orbital moment, we performed CI cluster calculation. The parameters of Os^{5+} are: U_{dd} = 1.0 eV, U_{cd} = 3.0 eV, Δ = 0.5, 10Dq = 3.2 eV, $pd\sigma$ = 2.43 eV, Slater integrals reduced to 80% of Hartree-Fock values. As shown in Fig. 2(b), the calculated spectra nicely reproduce the experiment [Fig. 2(a)]. The obtained orbital and spin moments from theoretic calculations are 0.18 μ_B and −2.29 μ_B, respectively.

One can observe that the orbital and spin moments from the sum rules are smaller than the CI calculations, on account that the experimental spectra of Os were obtained at 300 K where the magnetization does not reach its maximum. On the other hand, the m_{orb}/m_{spin} ratio, which is independent of the magnetization, is obtained to be −0.10 via

sum rules, which is in good agreement with the CI calculated value of −0.08.

In the theoretic calculations, the charge transfer energy Δ was set to 0.5 eV for Os^{5+}, denoting the strong hybridization between the high valence Os^{5+} and ligand oxygens. As a result, the formally high-valence Os^{5+} ion has considerable contents of $5d^4\underline{L}$ and $5d^5\underline{L}^2$ (where $\underline{L}$ denotes a ligand hole on the O 2*p* orbital) configurations in the ground state, rather than a pure $5d^3$ state. However, when we change Δ, the orbital moment of Os^{5+} only slightly changes, indicating that the covalent hybridization is not the major reason for the orbital moment of Os^{5+}.

If one considers only the t_{2g} orbitals, three spin-up electrons give rise to half-filled state, thus Os^{5+} cannot have orbital moment. However, if all the 5*d* orbitals are considered, the mixing between t_{2g} and e_g orbitals can lead to an unquenched orbital moment, especially for 5*d* element which possesses a sizable SOC. From the simulations of the experimental XMCD, we obtained $10Dq$ = 3.2 eV and SOC = 0.4 eV,[42–44] thus the orbital mixing of t_{2g} and e_g is expected. In order to figure out how SOC affects the orbital moment of Os^{5+}, we calculated the L_z as a function of SOC. As shown in Fig. 3(a), when SOC = 0, the L_z quenches to zero representing the case that all 5*d* electrons are constrained at the t_{2g} orbital. With SOC increasing, L_z also gradually increases. Fig. 3(b) displays the L_z as a function of $10Dq$ (SOC fixed to 0.4 eV). One can observe that with $10Dq$ increasing, L_z decreases. A zero L_z is expected when $10Dq$ is large enough compared to SOC, representing again only t_{2g} occupation. These results indicate clearly that the mixing between t_{2g} and e_g orbitals is responsible for the orbital moment of Os^{5+} in CCFOO.

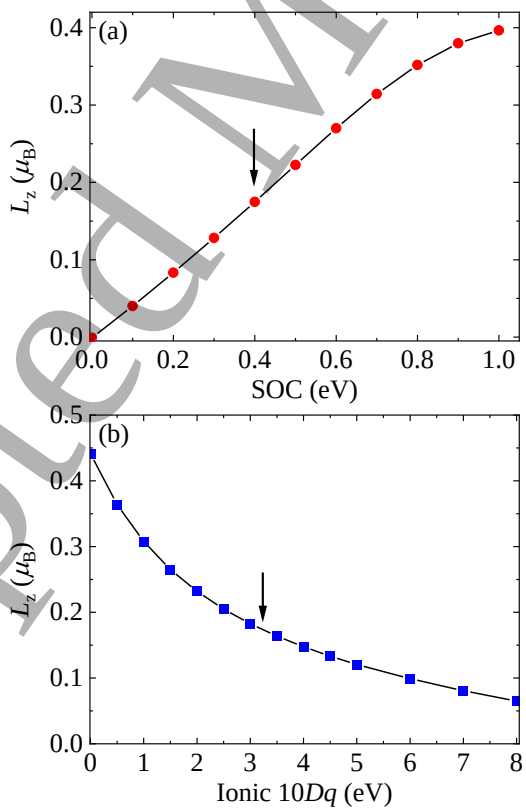

Fig. 3. L_z of Os^{5+} as a function of (a) SOC and (b) ionic $10Dq$. The arrows indicate the parameters of the calculated spectra in Fig. 2(b).

Now we turn to the Cu^{2+} at the A′ site. From Fig. 4(a) one can see that the XMCD signal at the Cu-L_3 edge is larger than that at the L_2 edge, indicating an unquenched orbital contribution of Cu^{2+} ion in CCFOO. Using sum rules we further obtained the m_{orb}, m_{spin} and m_{orb}/m_{spin} to be 0.06(3), 0.27(3) and 0.22, respectively, as listed in Table 1. Given that the orbital moment of Cu^{2+} ($3d^9$) is also unexpected for one e_g (x^2-y^2) occupation, we performed the CI cluster calculations for Cu^{2+}. The parameters are: U_{dd} = 8.0 eV, U_{cd} = 9.5 eV, Δ = 3.5 eV, total 10Dq = 1.65 eV, Δe_g = 2.99 eV, Δt_{2g} = 1.65 eV, V_{b1g} = 2.12 eV, V_{a1g} = 1.23 eV, V_{eg} = 0.80 eV, V_{b2g} = 1.13 eV, Slater integrals reduced to 80% of Hartree-Fock values. The crystal field parameters 10Dq, Δe_g and Δt_{2g} were obtained using the Madelung potential[45,46] based on the actual Cu^{2+} local structure,[17] which has a D_{4h} symmetry as shown in Fig. 1, and the hybridization parameters V_{b1g}, V_{a1g}, V_{eg} and V_{b2g} were obtained from Harrison's prescription.[47] The 10Dq = 1.65 eV of CCFOO is slightly smaller than experimental value 1.8 eV of La_2CuO_4[48] due to the longer Cu–O bond length (1.934 Å) in CCFOO than 1.90 Å in La_2CuO_4.[49]

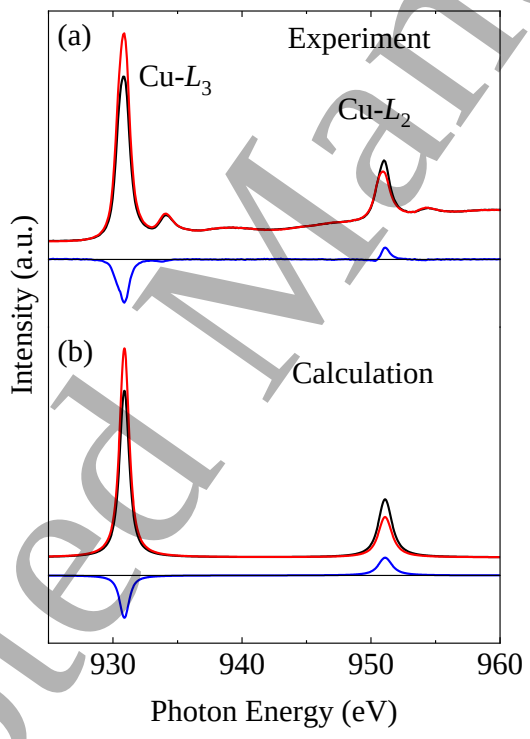

Fig. 4. (a) Experimental and (b) calculated XAS and XMCD spectra at the Cu-$L_{2,3}$ edges.

It is important to note that the A′ site Cu^{2+} forms a CuO_4 square planar (Fig. 1). Thus, we considered two configurations during the calculation: 1) beam incidence perpendicular to the plane and, 2) beam incidence parallel to the plane. The ratio of the two configurations is 1:2 for a polycrystalline sample. Fig. 4(b) displays our calculated Cu^{2+} spectra. The theoretic calculations give a nonnegligible orbital moment of 0.03 μ_B and a spin moment of 0.29 μ_B, with $L_z/2S_z$ = 0.10. Note that Cu is a late 3d TM, the 3d SOC of 0.10 eV is smaller than those of 5d elements, but not infinitely small as

compared with 10*Dq*. In consequence, SOC of 3*d* Cu leads to some degree of mixing of t_{2g} and e_g orbitals, which is responsible for a small but unquenched orbital moment.

The energy diagram of Cu^{2+} in CCFOO is depicted in Fig. 5(a). On account of the absence of the ligand oxygens at the *z* axis, the *z*-related orbitals are located at very low energies, resulting in a considerable splitting of both e_g and t_{2g} orbitals. In this case the hole is located at the x^2-y^2 orbital, thus the Cu^{2+} is not expected to have orbital moment. However, the mixing of x^2-y^2 and *xy* orbitals by SOC can result in a non-zero orbital moment. In order to confirm this, we also calculated the L_z of Cu^{2+} in CCFOO as a function of SOC and energy splitting of x^2-y^2 and *xy* orbitals (10*Dq*), as shown in Figs. 5(c) and 5(d), respectively. It clearly shows that, when SOC is ignored, Cu^{2+} does not have orbital moment. The orbital moment comes from the nonzero SOC as it is not infinitely small as compared with 10*Dq*. Our theoretic $L_z/2S_z$ value of 0.10 is smaller than the experiment (0.22). The discrepancy is ascribed to the small L_z value (0.06 μ_B) with an error bar (±0.03 μ_B) in the same order of magnitude of the sum rules.

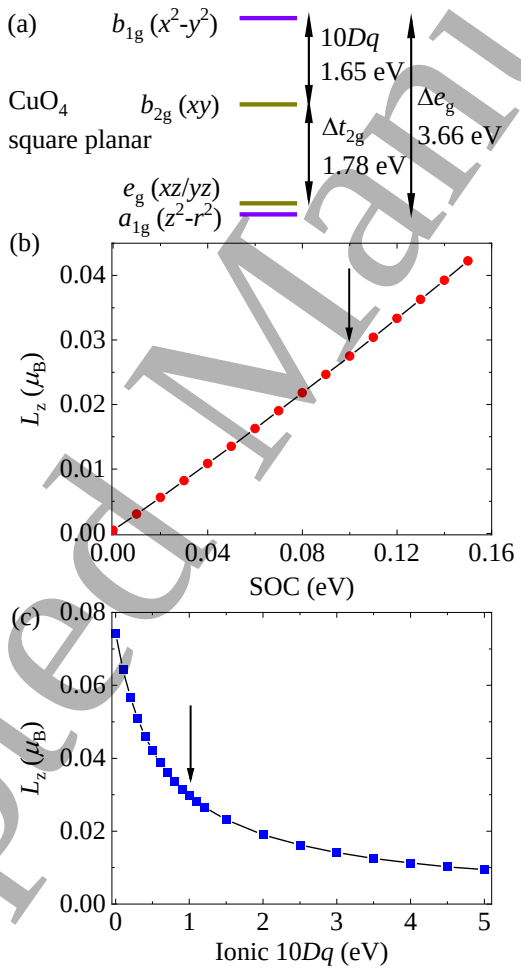

Fig. 5. (a) Orbital configuration of Cu^{2+} in CCFOO. L_z of Cu^{2+} as a function of (b) SOC and (c) ionic 10*Dq*. The arrows indicate the parameters of the calculated spectra in Fig. 4(b).

For Fe^{3+} XMCD, however, the sum rules are not applicable because of the significant overlap between the Fe-L_3 and -L_2 edges.[50] To obtain the correct spin moment from the experimental Fe-$L_{2,3}$ XMCD, we performed CI cluster calculations. The parameters are: U_{dd} = 7.5 eV, U_{cd} = 9.0 eV, Δ = 3.0 eV, 10Dq = 0.85 eV, $pd\sigma$ = 1.3 eV, Slater integrals reduced to 75% of Hartree-Fock values. An exchange field of 30 meV was applied.[16,51] The calculated XMCD signal is slightly larger than that of experimental owing to the Fe/Os antisite occupation in CCFOO.[16] As shown in Fig. 6(b), the calculation with 12% reduction of XMCD signal readily reproduces both the line shape and the intensity of the experimental [Fig. 6(a)], and yields a spin moment of 4.15 μ_B/atom, as listed in Table 1. Noting that the orbital moment of Fe^{3+} almost totally quenches due to the high spin $3d^5$ configuration with a fully occupied spin-up 3d shell and a fully empty spin-down 3d shell. Hereto, with theoretic calculations, we obtain a total moment of 5.0 μ_B/f.u. of CCFOO, in good agreement with the macroscopic magnetization (5.0 μ_B/f.u.).[16]

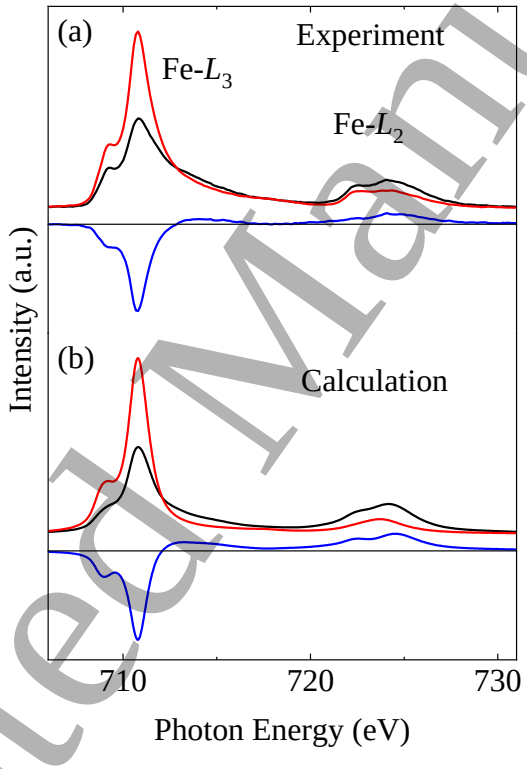

Fig. 6. (a) Experimental and (b) calculated XAS and XMCD spectra at the Fe-$L_{2,3}$ edges.

Our findings can also explain the magnetic behaviors in many other similar systems such as $CaCu_3Fe_2Re_2O_{12}$,[7] $CaCu_3Cr_2Re_2O_{12}$,[52] $NaCu_3Fe_2Re_2O_{12}$,[53] $NaCu_3Fe_2Os_2O_{12}$,[11] $LaCu_3Fe_{4-x}Os_xO_{12}$[20] and $CaCu_3Mn_2Os_2O_{12}$[20] with the A′-site Cu^{2+} and the same spin configuration [A′(↑)B(↑)B′(↓)] as which of CCFOO system. In these perovskite oxides, the orbital moment of B-site Fe^{3+}/$Mn^{3+/4+}$ is almost quenched and thus the A′-O-B′ coupling is the dominant magnetic coupling. It is reasonable to speculate that the orbital moments of Cu and Os/Re play critical roles in stabilizing the magnetic coupling and realizing a high Curie temperature close to and even much

higher than room temperature. On the other hand, however, when the B-site Fe^{3+} is replaced by Co^{2+} ($3d^7$) with a large orbital moment, the Cu(A′)-O-Co(B) AFM coupling is obviously enhanced, giving rise to strong magnetic frustration between the AFM coupled A′, B and B′ sites. In consequence, the T_C drastically decreases to 150 K for $LaCu_3Co_2Re_2O_{12}$[54] and 20 K for $CaCu_3Co_2Re_2O_{12}$.[55]

4. Conclusions

In conclusion, by performing both experimental sum rules and theoretical configuration interaction cluster calculations, the local states of all the transition metal cations, Cu, Fe and Os of the quadruple perovskite oxide $CaCu_3Fe_2Os_2O_{12}$ were investigated. The microsopic parameters such as crystal field, spin-orbit coupling (SOC), Coulomb potential and hybridization were obtained. Specifically, The Os^{5+} ($5d^3$) with a half-filled t_{2g} orbital exhibits a large orbital moment on account of the mixing of the t_{2g} and e_g orbitals, which can be ascribed to the strong SOC of the 5*d* elements. On the other hand, SOC of the 3*d* ion Cu^{2+} is markedly reduced, but is still nonnegligible compared to the crystal field 10*Dq*, leading to a finite orbital moment. In contrast, the orbital moment is close to zero for Fe^{3+}, with a half-filled 3*d* orbital. This work provides an element-selected perspective to investigate the microscopic and localized environment of the magnetic ions in complex oxides.

Acknowledgment

This work was supported by the High-Level Talent Research Start-Up Project Funding of Henan Academy of Sciences (Project No. 20251827005), the National Key R&D Program of China (Grant No. 2021YFA1400300), the National Natural Science Foundation of China (Grant Nos. 12425403, 12304159, 12261131499). The research in Dresden was partially supported by the DFG through SFB 1143.

References

1 Long Y W, Hayashi N, Saito T, Azuma M, Muranaka S and Shimakawa Y 2009 *Nature* **458** 60
2 Long Y W 2016 *Chin. Phys. B* **25** 078108
3 Sakai Y, Yang J, Yu R, *et al.* 2017 *J. Am. Chem. Soc.* **139** 4574
4 Liu Z, Sakai Y, Yang J, *et al.* 2020 *J. Am. Chem. Soc.* **142** 5731
5 Wang X, Chai Y, Zhou L, Cao H, Cruz C D, Yang J, Dai J, Yin Y, Yuan Z, Zhang S, Yu R, Azuma M, Shimakawa Y, Zhang H, Dong S, Sun Y, Jin C and Long Y 2015 *Phys. Rev. Lett.* **115** 087601
6 Zhou L, Dai J, Chai Y, Zhang H, Dong S, Cao H, Calder S, Yin Y, Wang X, Shen X, Liu Z, Saito T, Shimakawa Y, Hojo H, Ikuhara Y, Azuma M, Hu Z, Sun Y, Jin C and Long Y 2017 *Adv. Mater.* **29** 1703435
7 Liu G, Pi M, Zhou L, Liu Z, Shen X, Ye X, Qin S, Mi X, Chen X, Zhao L, Zhou B, Guo J, Yu X, Chai Y, Weng H and Long Y 2022 *Nat. Commun.* **13** 2373
8 Ye X, Yin Y, Cao Y, *et al.* 2025 *Nat. Commun.* **16** 3746
9 Zhang J, Ye X, Wang X, Pan Z, Pi M, Tang S, Dong C, Chen C T, Chen J M, Kuo C Y, Hu Z, Shen X, Yu X, Shen Y, Yu R and Long Y 2025 *J. Am. Chem. Soc.* **147**

12644
10 Chen W T, Mizumaki M, Seki H, Senn M S, Saito T, Kan D, Attfield J P and Shimakawa Y 2014 *Nat. Commun.* **5** 3909
11 Wang X, Liu M, Shen X, Liu Z, Hu Z, Chen K, Ohresser P, Nataf L, Baudelet F, Lin H J, Chen C T, Soo Y L, Yang Y F, Jin C and Long Y 2019 *Inorg. Chem.* **58** 320
12 Liu Z, Zhang S, Wang X, Ye X, Qin S, Shen X, Lu D, Dai J, Cao Y, Chen K, Radu F, Wu W B, Chen C T, Francoual S, Mardegan J R L, Leupold O, Tjeng L H, Hu Z, Yang Y f and Long Y 2022 *Adv. Mater.* **34** 2200626
13 Yamada I, Fujii H, Takamatsu A, Ikeno H, Wada K, Tsukasaki H, Kawaguchi S, Mori S and Yagi S 2017 *Adv. Mater.* **29** 1603004
14 Ye X, Song S, Li L, Chang Y C, Qin S, Liu Z, Huang Y C, Zhou J, Zhang L j, Dong C L, Pao C W, Lin H J, Chen C T, Hu Z, Wang J Q and Long Y 2021 *Chem. Mater.* **33** 9295
15 Sun N, Li W, Qin Y, Zheng Z, Zhang B, Dong X, Wei P, Zhang Y, He X, Xie X, Huang K, Wu L, Lei M, Gou H and Yu R 2024 *Chin. Phys. B* **33** 128101
16 Deng H, Liu M, Dai J, *et al.* 2016 *Phys. Rev. B* **94** 024414
17 Wang X, Liu Z, Deng H, Agrestini S, Chen K, Lee J F, Lin H J, Chen C T, Choueikani F, Ohresser P, Wilhelm F, Rogalev A, Tjeng L H, Hu Z and Long Y 2022 *Inorg. Chem.* **61** 16929
18 Thole B T, Carra P, Sette F and van der Laan G 1992 *Phys. Rev. Lett.* **68** 1943
19 Carra P, Thole B T, Altarelli M and Wang X 1993 *Phys. Rev. Lett.* **70** 694
20 Wang X, Liu Z, Hu Z, Ye X, Wang W, Yu R, Agrestini S, Zhou G, Chen K, Choueikani F, Ohresser P, Baudelet F, Lin H J, Chen C T, Tanaka A, Weng S C and Long Y 2021 *Inorg. Chem.* **60** 6298
21 Gao L, Wang X, Ye X, Wang W, Liu Z, Qin S, Hu Z, Lin H J, Weng S C, Chen C T, Ohresser P, Baudelet F, Yu R, Jin C and Long Y 2019 *Inorg. Chem.* **58** 15529
22 Ballhausen C J 1962 *Introduction to Ligand Field Theory* (McGraw-Hill, New York) pp. 113–151
23 Kim B J, Ohsumi H, Komesu T, Sakai S, Morita T, Takagi H and Arima T 2009 *Science* **323** 1329
24 Agrestini S, Kuo C Y, Chen K, Utsumi Y, Mikhailova D, Rogalev A, Wilhelm F, Förster T, Matsumoto A, Takayama T, Takagi H, Haverkort M W, Hu Z and Tjeng L H 2018 *Phys. Rev. B* **97** 214436
25 Kim B J, Jin H, Moon S J, Kim J Y, Park B G, Leem C S, Yu J, Noh T W, Kim C, Oh S J, Park J H, Durairaj V, Cao G and Rotenberg E 2008 *Phys. Rev. Lett.* **101** 076402
26 Yue Z L, Zhen W L, Niu R, Jiao K K, Zhu W K, Pi L and Zhang C J 2024 *Chin. Phys. B* **33** 017402
27 Cheng J G, Zhou J S, Yang Y F, Zhou H D, Matsubayashi K, Uwatoko Y, MacDonald A and Goodenough J B 2013 *Phys. Rev. Lett.* **111** 176403
28 Chen C T, Idzerda Y U, Lin H J, Smith N V, Meigs G, Chaban E, Ho G H, Pellegrin E and Sette F 1995 *Phys. Rev. Lett.* **75** 152
29 Burnus T, Hu Z, Wu H, Cezar J C, Niitaka S, Takagi H, Chang C F, Brookes N B, Lin H J, Jang L Y, Tanaka A, Liang K S, Chen C T and Tjeng L H 2008 *Phys. Rev. B* **77** 205111
30 Agrestini S, Chen K, Kuo C Y, Zhao L, Lin H J, Chen C T, Rogalev A, Ohresser P, Chan T S, Weng S C, Auffermann G, Völzke A, Komarek A C, Yamaura K, Haverkort M W, Hu Z and Tjeng L H 2019 *Phys. Rev. B.* **100** 014443
31 Chen J, Wang X, Hu Z, Tjeng L H, Agrestini S, Valvidares M, Chen K, Nataf L,

Baudelet F, Nagao M, Inaguma Y, Belik A A, Tsujimoto Y, Matsushita Y, Kolodiazhnyi T, Sereika R, Tanaka M and Yamaura K 2020 *Phys. Rev. B* **102** 184418
32 Feng H L, Chen J, Hu Z, Wang X, Reehuis M, Adler P, Hoser A, Wu M X, Agrestini S, Vasili H B, Herrero-Martin J, Nataf L, Baudelet F, Chen K, Matsushita Y, Li M R, Tjeng L H, Felser C, Jansen M and Yamaura K 2020 *Phys. Rev. Mater.* **4** 064420
33 Stöhr J and König H 1995 *Phys. Rev. Lett.* **75** 3748
34 Teramura Y, Tanaka A and Jo T 1996 *J. Phys. Soc. Jpn.* **65** 1053
35 Zaanen J, Sawatzky G A and Allen J W 1985 *Phys. Rev. Lett.* **55** 418
36 He Y, Fecher G H, Kroder J, Borrmann H, Wang X, Zhang L, Kuo C Y, Liu C E, Chen C T, Chen K, Choueikani F, Ohresser P, Tanaka A, Hu Z and Felser C 2020 *Appl. Phys. Lett.* **116** 102404
37 Wang X, Hu Z, Agrestini S, Herrero-Martín J, Valvidares M, Sankar R, Chou F C, Chu Y H, Tanaka A, Tjeng L H 2021 *J. Magn. Magn. Mater.* **530** 167940
38 Li L, Zhou J, Wang X, Gracia J, Valvidares M, Ke J, Fang M, Shen C, Chen J M, Chang Y C, Pao C W, Hsu S Y, Lee J F, Ruotolo A, Chin Y, Hu Z, Huang X and Shao Q 2023 *Adv. Mater.* **35** 2302966
39 Zhao J, Hao S C, Wang X, Cao L, Lin H J, Chen C T, Sahle C J, Tanaka A, Chen J M, Jin C, Hu Z and Tjeng L H 2023 *Phys. Rev. B* **107** 024107
40 Wang X, Zhang J, Pan Z, Lu D, Pi M, Ye X, Dong C, Chen J, Chen K, Radu F, Francoual S, Agrestini S, Hu Z, Chang C F, Tanaka A, Yamaura K, Shen Y and Long Y 2024 *J. Phys. Chem. C* **128** 15668
41 Tanaka A and Jo T 1994 *J. Phys. Soc. Jpn.* **63** 2788
42 Taylor A E, Calder S, Morrow R, Feng H L, Upton M H, Lumsden M D, Yamaura K, Woodward P M and Christianson A D 2017 *Phys. Rev. Lett.* **118** 207202
43 Yuan B, Clancy J P, Cook A M, Thompson C M, Greendan J, Cao G, Jeon B C, Noh T W, Upton M H, Casa D, Gog T, Paramekanti A and Kim Y J 2017 *Phys. Rev. B* **95** 235114
44 Paramekanti A, Singh D J, Yuan B, Casa D, Said A, Kim Y J and Christianson A D 2018 *Phys. Rev. B* **97** 235119
45 Chin Y Y, Lin H J, Hu Z, Kuo C Y, Mikhailova D, Lee J M, Haw S C, Chen S A, Schnelle W, Ishii H, Hiraoka N, Liao Y F, Tsuei K D, Tanaka A, Tjeng L H, Chen C T and Chen J M 2017 *Sci. Rep.* **7** 3656
46 Chin Y Y, Hu Z, Su Y, Tsujimoto Y, Tanaka A and Chen C T 2018 *Phys. Status Solidi RRL* **12** 1800147
47 Harrsion W A 1989 *Electronic Structure and the Properties of Solids* (Dover Publications Inc.) pp. 552–553
48 Sala M M, Bisogni V, Aruta C, Balestrino G, Berger H, Brookes N B, de Luca G M, Castro D D, Grioni M, Guarise M, Medaglia P G, Granozio F M, Minola M, Perna P, Radovic M, Salluzzo M, Schmitt T, Zhou K J, Braicovich L and Ghiringhelli G 2011 *New. J. Phys.* **13** 043026
49 Longo J M and Raccah P M 1973 *J. Solid State Chem.* **6** 526
50 Piamonteze C, Miedema P and de Groot F M F 2009 *Phys. Rev. B* **80** 184410
51 Alders D, Tjeng L H, Voogt F C, Hibma T, Sawatzky G A, Chen C T, Vogel J, Sacchi M and Iacobucci S 1998 *Phys. Rev. B* **57** 11623
52 Zhang J, Liu Z, Ye X, Wang X, Lu D, Zhao H, Pi M, Chen C T, Chen J L, Kuo C Y, Hu Z, Yu X, Zhang X, Pan Z and Long Y 2024 *Inorg. Chem.* **63** 3499
53 Zhang J, Temnikov F, Ye X, Wang X, Pan Z, Liu Z, Pi M, Tang S, Chen C T, Pao C W, Huang W H, Kuo C Y, Hu Z, Shen Y, Streltsov S V and Long Y 2025 *Inorg. Chem.* **64** 472

54 Liu Z, Sun Q, Ye X, Wang X, Zhou L, Shen X, Chen K, Nataf L, Baudelet F, Agrestini S, Chen C T, Lin H J, Vasili H B, Valvidares M, Hu Z, Yang Y f and Long Y 2020 *Appl. Phys. Lett.* **117** 152402
55 Liu Z, Wang X, Ye X, *et al.* 2021 *Phys. Rev. B* **103** 014414